

Systems Science & Control Engineering

An Open Access Journal

ISSN: (Print) (Online) Journal homepage: <https://www.tandfonline.com/loi/tssc20>

Maximum torque per ampere and maximum power per ampere sliding mode control for interior permanent magnet synchronous motors

Hashim Alnami, Chengzong Pang, Avinash Papineni & Xin Wang

To cite this article: Hashim Alnami, Chengzong Pang, Avinash Papineni & Xin Wang (2021) Maximum torque per ampere and maximum power per ampere sliding mode control for interior permanent magnet synchronous motors, *Systems Science & Control Engineering*, 9:1, 704-713, DOI: [10.1080/21642583.2021.1989635](https://doi.org/10.1080/21642583.2021.1989635)

To link to this article: <https://doi.org/10.1080/21642583.2021.1989635>



© 2021 The Author(s). Published by Informa UK Limited, trading as Taylor & Francis Group



Published online: 14 Oct 2021.



Submit your article to this journal [↗](#)



Article views: 62



View related articles [↗](#)



View Crossmark data [↗](#)

Maximum torque per ampere and maximum power per ampere sliding mode control for interior permanent magnet synchronous motors

Hashim Alnami^a, Chengzong Pang^a, Avinash Papineni^b and Xin Wang^b

^aSchool of Electrical Engineering and Computer Science, Wichita State University, Wichita, KS, USA; ^bDepartment of Electrical and Computer Engineering, Southern Illinois University, Edwardsville, IL, USA

ABSTRACT

This paper presents novel maximum torque per ampere (MTPA) and maximum power per ampere (MPPA) sliding mode control (SMC) approaches for interior permanent-magnet synchronous motors (IPMs). We first derive the first-order SMC methods to improve the field-oriented control's resiliency against the external perturbations, extraneous noise and modelling uncertainties. After that, we propose the higher-order SMC to significantly reduce the chattering phenomenon, which is inherent in the first-order sliding mode method. Based on the comparison studies, the conventional proportional-integral-derivative based field oriented control shows sluggish response and is more sensitive to parameter perturbations and external torque disturbances. By introducing the novel SMC methods, both the speed and torque regulation performance of interior permanent magnet synchronous motor can be greatly improved. Computer simulation studies have demonstrated the superior performance of the first-order and higher-order sliding mode controllers for interior permanent magnet synchronous motor speed and torque regulation applications.

ARTICLE HISTORY

Received 6 April 2021
Accepted 2 October 2021

KEYWORDS

Permanent magnet synchronous motors; field oriented control; sliding mode control

1. Introduction

Permanent magnet synchronous motors (PMs) have been widely used for industrial applications due to their large torque to inertia ratio, high power density, high power factor, extended bearing and efficient insulation life time, superior energy efficiency and great dependability.

In field-oriented control method, i_d is set to zero to avoid demagnetization effect. With the introduction of permanent magnets of high coercive forces, there is no need to bound to this method. The competence of IPM motor along with demanded inverter capacity depends on the current phase control methods, i.e. controlling the phase angle β of armature current. The current phase control methods are $i_d = 0$ control method, $\cos \phi = 1$ control method and constant flux linkage control method. The $i_d = 0$ method is used for surface-mounted motor as torque is linear to armature current, high torque performance is obtained and no demagnetization effect is seen. In $\cos \phi = 1$ control method, torque per armature current is small and torque is non-linear in nature, hence its best suitable for constant speed drive applications. Constant flux linkage method gives torque characteristics closer to linear and required

inverter capacity is small, hence its best suited for interior permanent magnet synchronous motor Uddin et al. (2002).

In conventional DC motors, magnetic flux can be directly reduced to increase the speed operation range. However, for permanent magnet synchronous motors, air gap flux needs to be decreased by direct-axis armature current. This method is commonly known as 'flux-weakening'. Morimoto et al. conducted experiments in which several motor parameters were examined under wide-speed operation range and the results are summarized as follows (Morimoto et al., 1993; Morimoto, Sanada et al., 1994; Morimoto et al., 1990a, 1990b):

- The operating limits can be increased by controlling the d and q axis armature currents according to rotor speed.
- If the supply voltage is less than rated voltage, operating region can be large. If both are equal, ideal output characteristics can be obtained. However, if the power supply voltage is less than rated voltage, then at low speed range, the output power can be large, but wide-speed operation is not possible.

CONTACT Xin Wang  xwang@siue.edu

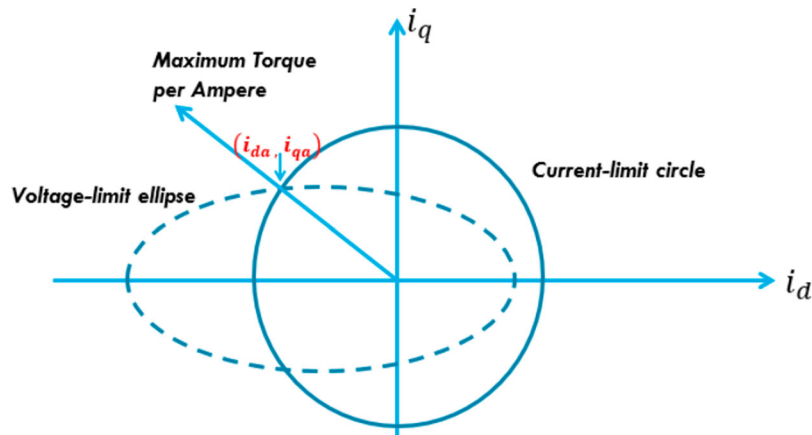


Figure 1. MTPA and MPPA trajectory.

- Due to the saliency, IPM motor has additional torque component called reluctance torque. Hence, the output torque can be large.
- In the constant power regions, permanent magnet with high coercivity and linear demagnetization curve should be used.

The flux weakening control is used for constant power operation. Due to saliency in IPM motor, reluctance torque can be productively used by MTPA control to generate large torque. Several characteristics such as torque, power factor, efficiency, and transient response are examined and are compared with $i_d = 0$ control method. By controlling d -axis, current torque per ampere is large and power factor is improved compared to $i_d = 0$ method.

Traditional Proportional-Integral (PI)-based control techniques are still the most widely utilized method due to the ease of implementation and simplicity. However, it is sensitive to uncertainties and disturbance. Therefore, nonlinear and robust control techniques were proposed and implemented to boost the permanent magnet synchronous motor control performance.

To improve the traditional PI-based field-oriented control, various advanced control approaches have been developed, including sliding mode control (SMC), model predictive control, adaptive control and H_∞ robust control, intelligent control. The SMC is one of the most promising next-generation control scheme for power electronics and power systems. The philosophy behind SMC is to design a function called sliding variable which becomes zero on the sliding manifold. The systems performance depends on the proper selection of sliding variables Utkin et al. (1999). SMC guides the trajectory of the system to the sliding surface and keeps the movement of trajectory along the surface with the switching control law. The advantages with sliding

mode are its superior resiliency to external disturbances and perturbations, high accuracy and fast dynamic response.

SMC design is a two-step procedure: The first step is to choose a control law, which will steer the systems state to sliding surface even during troublesome environments. And the second step is to create a switching function that keeps the system trajectory on the sliding surface satisfying the design specifications. The first-order SMC is ineffective in eliminating the unwanted phenomenon chattering. This phenomenon occurs due to non-ideal switching devices and time delays in processors. The higher-order SMC for PM motors was presented in Levant and Fridman (2002) and higher-order observer of PM motor was implemented in Xu and Rahman (2003). The higher-order SMC has been the preferred approach, since it is more effective in eliminating chattering phenomenon and achieving superior dynamic performance (Wang et al., 2016, 2018).

Leveraging our previous effort in Alnami et al. (2021), in this paper, novel first-order and super-twisting-based second-order SMC for interior permanent magnet synchronous motor drives are derived. The interior permanent magnet synchronous motor drives, which have been widely used for modern electrified vehicles, can achieve maximum torque per ampere (MTPA) and maximum power per ampere (MPPA) performance via the proposed SMC methods, as illustrated in Figure 1. The conditions for MTPA and MPPA control of IPMs are derived in this paper. In addition, both control methods are compared with the traditional PI control for the MTPA and MPPA control of IPMs. While both sliding methods show exceptional performance in transient response, guaranteed Lyapunov stability, robustness against the modelling uncertainties and extraneous disturbances, the second-order SMC is superior in eliminating the chattering phenomenon which is inherent in the first-order approach.

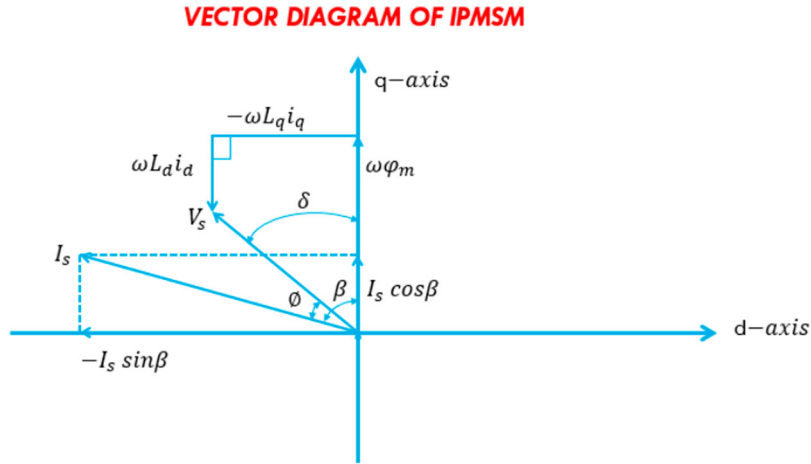


Figure 2. IPM's vector diagram.

This paper is organized as follows: Section 2 provides dynamical model of IPMs. Sections 3 and 4 present the direct-axis reference current i_d 's derivations, conditions to apply MTPA and MPPA, disadvantages of PI controller, advantages of SMC. In Section 5, first-order SMC is proposed. Section 5 also presents the design of the super-twisting-based second-order SMC. Section 6 explains the computer simulation results. Section 7 concludes the paper.

2. Interior permanent magnet synchronous motor model

The direct and quadrature axis stator voltage equation in the dq coordinates frame can be described as Krause et al. (2013)

$$\begin{bmatrix} v_d \\ v_q \end{bmatrix} = \begin{bmatrix} R + \frac{d}{dt}L_d & -\omega L_q \\ \omega L_d & R + \frac{d}{dt}L_q \end{bmatrix} \begin{bmatrix} i_d \\ i_q \end{bmatrix} + \begin{bmatrix} 0 \\ \omega \Psi_m \end{bmatrix} \quad (1)$$

Equation (1) can be expressed in current frame of reference as

$$\frac{di_d}{dt} = \frac{1}{L_d} \left[-R i_d + \frac{P}{2} \omega_r L_q i_q + v_d \right] \quad (2)$$

$$\frac{di_q}{dt} = \frac{1}{L_q} \left[-R i_q - \frac{P}{2} \omega_r (L_d i_d + \Psi_m) + v_q \right] \quad (3)$$

where i_d represents the direct-axis current, i_q stands for the quadrature-axis current, R is the resistance of the stator, rotor mechanical speed is ω_r , L_d and L_q denote the direct-axis and quadrature-axis inductance, respectively.

The mechanical equation can be written as

$$\frac{d\omega_r}{dt} = \frac{\tau_{em}}{J} - \frac{\tau_m}{J} - \frac{B\omega_r}{J} \quad (4)$$

where B represents the damping coefficient, J denotes the moment of inertia, τ_m is the mechanical torque, where

the number of poles is P , and Ψ_m represents the flux linkage. And τ_{em} denotes the electromagnetic torque satisfies

$$\tau_{em} = \frac{3P}{4J} [\Psi_m i_q + (L_d - L_q) i_d i_q] \quad (5)$$

Notice that ω and ω_r are the electrical and mechanical speed, respectively. The relation between electrical and mechanical rotor speed is

$$\omega = \frac{P}{2} \omega_r \quad (6)$$

The direct i_d and i_q currents can be represented in terms of armature current and phase angle as follows:

$$\begin{aligned} i_d &= -I_a \sin \beta \\ i_q &= I_a \cos \beta \end{aligned} \quad (7)$$

where I_a is the magnitude of armature current per phase. β is the leading angle of armature current vector from the q axis, as shown in Figure 2.

The torque τ_{em} can be represented as

$$\tau_{em} = \frac{3P}{2} [\Psi_m I_a \cos \beta + 0.5(L_q - L_d) I_a^2 \sin 2\beta] \quad (8)$$

3. Maximum torque per ampere (MTPA)

The maximum torque point τ_{max} can be reached at intersection point between current-limit circle and MTPA's trajectory as shown in Figure 3.

Direct-axis and quadrature-axis current need to be derived by taking the derivative of developed torque with respect to β and equating it to zero.

$$\frac{d\tau_{em}}{d\beta} = \frac{3P}{4} [-\Psi_m I_a \sin \beta + (L_q - L_d) I_a^2 \cos 2\beta] = 0 \quad (9)$$

After simplification, Equation (9) can be rewritten as

$$2(L_q - L_d) I_a \sin^2 \beta + \Psi_m \sin \beta - (L_q - L_d) I_a = 0 \quad (10)$$

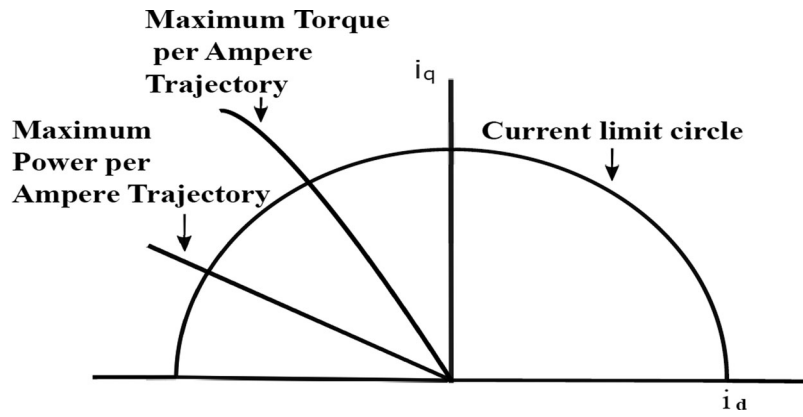


Figure 3. MTPA's trajectory.

Therefore, angle β can be calculated by

$$\beta = \sin^{-1} \left[\frac{-\Psi_m + \sqrt{\Psi_m^2 + 8(L_q - L_d)^2 I_a^2}}{4(L_q - L_d)I_a} \right] \quad (11)$$

The reference direct-axis current i_d^* and quadrature-axis current i_q^* can be calculated by substituting Equation (11) into Equation (7) as

$$i_d^* = -I_a \frac{-\Psi_m + \sqrt{\Psi_m^2 + 8(L_q - L_d)^2 I_a^2}}{4(L_q - L_d)I_a} \quad (12)$$

After simplification, i_d^* can be written as

$$i_d^* = \frac{\Psi_m}{4(L_q - L_d)} - \sqrt{\frac{\Psi_m^2}{16(L_q - L_d)^2} + \frac{I_a^2}{2}} \quad (13)$$

4. Maximum power per ampere (MPPA)

When the motor speed is greater than the rated speed, the current vector producing τ_{\max} cannot satisfy the voltage constraint above the rated speed. The d - and q -axis armature current components are controlled in order to keep the rated voltage V_0 equal to supply voltage in the flux-weakening constant power region. The relationship between i_d and i_q of the flux-weakening control is derived as follows:

$$V_0 = \sqrt{v_{d0}^2 + v_{q0}^2} \quad (14)$$

with

$$\begin{aligned} v_{d0} &= -\omega L_q i_q \\ v_{q0} &= \omega \Psi_m + \omega L_d i_d \end{aligned} \quad (15)$$

Equivalently, we have

$$V_0^2 = (-\omega L_q i_q)^2 + (\omega \Psi_m + \omega L_d i_d)^2 \quad (16)$$

Therefore, the reference direct-axis stator current can be calculated by:

$$i_d^* = \frac{-2\omega^2 \Psi_m L_d + \sqrt{(2\omega V_0 L_d)^2 - (2\omega^2 L_d L_q i_q)^2}}{2\omega^2 L_d^2} \quad (17)$$

which can be further simplified as

$$i_d^* = \frac{-\Psi_m}{L_d} + \frac{1}{L_d} \sqrt{\frac{V_0^2}{\omega^2} - (L_q i_q)^2} \quad (18)$$

When the motor speed is less than the rated speed, MTPA control is utilized. And when rotor speed is greater than the rated speed, MPPA control is applied. Classical PI controllers are used in the traditional field oriented control for motor speed and torque regulation. The traditional field oriented control uses space vector pulse width modulation (SVPWM) techniques to obtain the required voltage from inverter to the IPM motor. The currents from an IPM are converted from abc frame of reference to $\alpha\beta$ frame using Clarke's transformation and to dq frame of reference using Park's transform. The PI controllers requires decoupling stage and back-emf compensation. By performing decoupling, the two inputs v_d, v_q serves as the input signals to SVPWM.

5. Sliding mode control

SMC is a nonlinear control method which enjoys inherent robustness, flexibility of design and the ease to be implemented with microprocessors. The complete detailed analysis of SMC can be found in Wang et al. (2018).

Consider a nonlinear system

$$\dot{x}(t) = g(x(t)) + h(x(t))u(t) \quad (19)$$

where $x(t)$ is state variable, $g(\cdot)$ and $h(\cdot)$ are vector fields in the same space and $u(t)$ is the discontinuous control defined as

$$u(t) = \begin{cases} U^+ & s(x, t) > 0 \\ U^- & s(x, t) < 0 \end{cases}$$

where $s(x)$ is sliding variable and chosen such that state variables follow their desired trajectories. U^+ and U^- are function of $x(t)$. A system exhibits SMC when the reachability, existence and stability conditions are met.

The reachability conditions make the trajectories of system reach the sliding surface.

Mathematically, it can be defined as

$$s(x)\dot{s}(x) < 0 \quad (20)$$

The existence condition always direct the trajectory towards sliding surface, which can be stated as

$$\lim_{x \rightarrow \infty} s(x)\dot{s}(x) < 0 \quad (21)$$

The stability condition ensures the sliding surface directs trajectory towards stable equilibrium.

5.1. Sliding surfaces

Consider the following slide manifolds:

$$s_d = i_d - i_d^* = 0 \quad (22)$$

$$s_q = i_q - i_q^* = 0 \quad (23)$$

$$s_{\omega_r} = i_{\omega_r} - i_{\omega_r}^* = 0 \quad (24)$$

5.2. Parameter uncertainties

Due to unmodelled dynamics present in the mathematical model of an IPM, R is defined as $\hat{R} + \Delta R$, where \hat{R} is nominal resistance and ΔR is a bounded disturbance. Similarly, $L = \hat{L} + \Delta L$, $\Psi_m = \hat{\Psi}_m + \Delta \Psi_m$, $\tau_m = \hat{\tau}_m + \Delta \tau_m$, $J = \hat{J} + \Delta J$, and $B = \hat{B} + \Delta B$.

5.3. First-Order sliding mode control design

5.3.1. First-order flux sliding mode control

The direct-axis flux control is given as

$$v_d = v_{d,eq} + v_{d,N} \quad (25)$$

where $v_{d,eq}$ is the equivalent control and $v_{d,N}$ is the switching control. The equivalent control can be solved by taking derivative of $s_d = 0$.

$$\dot{s}_d = \frac{1}{L_d} \left[-Ri_d + \frac{P}{2} w_r L_q i_q + v_d - L_d \frac{di_d^*}{dt} \right] \quad (26)$$

Hence, the equivalent control $v_{d,eq}$ can be calculated as

$$v_{d,eq} = \left[\hat{R}i_d - \frac{P}{2} w_r \hat{L}_q i_q + \hat{L}_d \frac{di_d^*}{dt} \right] \quad (27)$$

\dot{s}_d can be rewritten as

$$\dot{s}_d = \frac{1}{L_d} \left[-\Delta R i_d - \Delta L_d \frac{di_d^*}{dt} + \Delta L_q \frac{P}{2} i_q w_r \right] + \frac{1}{L_d} v_{d,N} \quad (28)$$

Due to the uncertainties present in model parameters, there exists a positive constant u_{d0} such that

$$v_{d0} > |\Delta R i_d + \Delta L_d \frac{di_d^*}{dt} - \Delta L_q \frac{P}{2} i_q w_r| \quad (29)$$

Then v_d 's switching control component can be defined as

$$v_{d,N} = -v_{d0} \text{sgn}(s_d) \quad (30)$$

5.3.2. First-order torque sliding mode control

The quadrature axis torque control is given as

$$v_q = v_{q,eq} + v_{q,N} \quad (31)$$

where $v_{q,eq}$ is the equivalent control and $v_{q,N}$ is the switching control. The equivalent control can be solved by taking derivative of $s_q = 0$.

$$\dot{s}_q = \frac{1}{L_q} \left[-Ri_q - \frac{P}{2} w_r (L_d i_d + \Psi_m) + v_q - L_q \frac{di_q^*}{dt} \right] \quad (32)$$

Hence, the equivalent control $v_{q,eq}$ can be calculated as

$$v_{q,eq} = \left[\hat{R}i_q + \frac{P}{2} w_r (\hat{L}_d i_d + \hat{\Psi}_m) + \hat{L}_q \frac{di_q^*}{dt} \right] \quad (33)$$

\dot{s}_q can be rewritten as

$$\dot{s}_q = \frac{1}{L_q} \left[-\Delta R i_q - \frac{P}{2} w_r (\Delta L_d i_d + \Delta \Psi_m) + v_{q,N} - \Delta L_q \frac{di_q^*}{dt} \right] \quad (34)$$

Due to the uncertainties present in model parameters, there exists a positive constant u_{q0} such that

$$v_{q0} > |\Delta R i_q + \frac{P}{2} w_r (\Delta L_d i_d + \Delta \Psi_m) + \Delta L_q \frac{di_q^*}{dt}| \quad (35)$$

Then v_q 's switching control component can be defined as

$$v_{q,N} = -v_{q0} \text{sgn}(s_q) \quad (36)$$

5.3.3. First-Order speed sliding mode control

The first-order speed SMC is

$$i_q^* = i_{q,eq}^* + i_{q,N}^* \quad (37)$$

where $i_{q,eq}$ is the equivalent control and $i_{q,N}$ is the switching control. The equivalent control can be solved by taking derivative of $s_{wr} = 0$.

$$\dot{s}_{wr} = \frac{3P}{4J} [\Psi_m i_q + (L_d - L_q) i_d i_q] - \frac{\tau_m}{J} - \frac{B w_r}{J} - \frac{dw_r^*}{dt} \quad (38)$$

Hence, the equivalent control can be calculated as

$$i_{q,eq}^* = \frac{1}{K_t} \left[\hat{\tau}_m + \hat{B}w_r + \hat{J} \frac{dw_r^*}{dt} \right] \quad (39)$$

with

$$K_t = \frac{3P}{4} [\Psi_m + (L_d - L_q)i_d] \quad (40)$$

Due to the uncertainties present in model parameters, there exist a positive constant i_{q0} such that

$$i_{q0} > \left| \frac{1}{K_t} \left[\Delta \tau_m + \Delta Bw_r + \Delta J \frac{dw_r^*}{dt} \right] \right| \quad (41)$$

Then i_q 's switching control component can be defined as

$$i_{q,N} = -i_{q0} \text{sgn}(s_{wr}) \quad (42)$$

5.4. Super twisting algorithm based higher-Order sliding mode control design

Applying the first-order SMC is known to have an undesirable performance limitation known as the chattering phenomenon. Chattering, often caused by the non-ideal switching devices and the time delays in microprocessors, is a high-frequency movement which makes the state trajectories quickly oscillating around the sliding surface. If chattering phenomenon is severe, it can cause performance degradation in the control system effectiveness or even may lead to damage or failures of the system. To address this limitation, we propose the complete derivations of the higher-order SMC based on the super-twisting algorithm. For higher-order SMC approach, the sliding surfaces and the equivalent controls are kept the same as in the first-order SMC approach.

5.4.1. Higher-order flux sliding mode control

In the second-order flux SMC, the sliding manifold $s_d(x)$ and its first-order derivative $\dot{s}_d(x)$ must be driven to zero. Hence, we have

$$\dot{s}_d = \frac{1}{L_d} \left[-Ri_d + \frac{P}{2} w_r L_q i_q + v_d - L_d \frac{di_d^*}{dt} \right] \quad (43)$$

and

$$\ddot{s}_d = \frac{-R}{L_d} \frac{di_d}{dt} + \frac{L_q P}{L_d 2} \left(\frac{dw_r}{dt} i_q + \frac{di_q}{dt} w_r \right) + \frac{1}{L_d} \frac{dv_d}{dt} - \frac{d^2 i_d^*}{dt^2} \quad (44)$$

Let's denote

$$\psi_d = \frac{-R}{L_d} \frac{di_d}{dt} + \frac{L_q P}{L_d 2} \frac{dw_r}{dt} i_q + \frac{L_q P}{L_d 2} \frac{di_q}{dt} w_r - \frac{d^2 i_d^*}{dt^2} \in [-\Psi_d, \Psi_d] \quad (45)$$

and

$$\gamma_d = \frac{1}{L_d} \in [\Gamma_m, \Gamma_M] \quad (46)$$

v_d is the control input which is combination of the equivalent control $v_{d,eq}$ and switching control \tilde{v}_d .

$$\tilde{v}_d = v_{d1} + v_{d2} \quad (47)$$

where

$$v_{d1} = -W_d \text{sgn}(s_d) \quad (48)$$

$$v_{d2} = \begin{cases} -\lambda_d |s_0|^p \text{sgn}(s_d) & |s_d| > |s_0| \\ -\lambda_d |s_d|^p \text{sgn}(s_d) & |s_d| \leq |s_0| \end{cases}$$

The sufficient conditions for finite-time convergence to the sliding manifold can be described as

$$W_d > \frac{\Psi_d}{\Gamma_m} \quad (49)$$

$$\lambda_d^2 \geq \frac{4\Psi_d}{\Gamma_m^2} \frac{\Gamma_M(W_d + \Psi_d)}{\Gamma_m(W_d - \Psi_d)} \quad (50)$$

$$0 < p \leq 0.5 \quad (51)$$

By selecting $p = 0.5$, we can reach the switching control as

$$\tilde{v}_d = -\lambda_d |s_d|^{1/2} \text{sgn}(s_d) - W_d \int \text{sgn}(s_d) dt \quad (52)$$

5.4.2. Higher-order torque sliding mode control

By adopting a similar approach, in the second-order torque SMC design, the sliding manifold $s_q(x)$ and its first-order derivative $\dot{s}_q(x)$ must be driven to zero. Hence, we have

$$\dot{s}_q = \frac{1}{L_q} \left[-Ri_q - \frac{P}{2} w_r (L_d i_d + \Psi_m) + v_q - L_q \frac{di_q^*}{dt} \right] \quad (53)$$

and

$$\ddot{s}_q = \frac{-R}{L_q} \frac{di_q}{dt} - \frac{P L_d}{2 L_q} \left(\frac{di_d}{dt} w_r + \frac{dw_r}{dt} i_d \right) - \frac{P}{2} \frac{dw_r}{dt} \frac{\Psi_m}{L_q} + \frac{1}{L_q} \frac{dv_q}{dt} - L_q \frac{d^2 i_q^*}{dt^2} \quad (54)$$

Let us denote

$$\psi_q = \frac{-R}{L_q} \frac{di_q}{dt} - \frac{P L_d}{2 L_q} \left(\frac{di_d}{dt} w_r + \frac{dw_r}{dt} i_d \right) - \frac{P}{2} \frac{dw_r}{dt} \frac{\Psi_m}{L_q} - L_q \frac{d^2 i_q^*}{dt^2} \in [-\Psi_q, \Psi_q] \quad (55)$$

and

$$\gamma_q = \frac{1}{L_q} \in [\Gamma_m, \Gamma_M] \quad (56)$$

v_q is the control input, which is the combination of equivalent control $v_{q,eq}$ and switching control \tilde{v}_q .

$$\tilde{v}_q = v_{q1} + v_{q2} \quad (57)$$

where

$$\dot{v}_{q1} = -W_q \text{sgn}(s_q) \quad (58)$$

$$u_{q2} = \begin{cases} -\lambda |s_q|^p \text{sgn}(s_q) & |s_q| > |s_0| \\ -\lambda |s_q|^p \text{sgn}(s_q) & |s_q| \leq |s_0| \end{cases}$$

The sufficient condition for finite time convergence to the sliding manifold can be described as

$$W_q > \frac{\Psi_q}{\Gamma_m} \quad (59)$$

$$\lambda_q^2 \geq \frac{4\Psi_q}{\Gamma_m^2} \frac{\Gamma_M(W_q + \Psi_q)}{\Gamma_m(W_q - \Psi_q)} \quad (60)$$

$$0 < p \leq 0.5 \quad (61)$$

By selecting $p = 0.5$, we can reach the switching control as

$$\tilde{v}_q = -\lambda_q |s_q|^{1/2} \text{sgn}(s_q) - W_q \int \text{sgn}(s_q) dt \quad (62)$$

5.4.3. Higher-order speed sliding mode control

Again, in the second-order speed SMC design, the sliding manifold $s_{wr}(x)$ and its first-order derivative $\dot{s}_{wr}(x)$ must be driven to zero. Hence, we have

$$\dot{s}_{wr} = \frac{3P}{4J} [\Psi_m i_q + (L_d - L_q) i_d i_q] - \frac{\tau_m}{J} - \frac{B w_r}{J} - \frac{d w_r^*}{dt} \quad (63)$$

and

$$\ddot{s}_{wr} = -\frac{1}{J} \frac{d\tau_m}{dt} + \frac{K_t}{J} \frac{di_q}{dt} - \frac{B}{J} \frac{dw_r}{dt} - \frac{d^2 w_r^*}{dt^2} \quad (64)$$

Let's denote

$$\psi_w = -\frac{1}{J} \frac{d\tau_m}{dt} - \frac{B}{J} \frac{dw_r}{dt} - \frac{d^2 w_r^*}{dt^2} \in [-\Psi_w, \Psi_w] \quad (65)$$

and

$$\gamma_w = \frac{K_t}{J} \in [\Gamma_m, \Gamma_M] \quad (66)$$

i_q^* is the input control, which is the combination of equivalent control $i_{q,eq}^*$ and switching control \tilde{i}_q^* .

$$i_q^* = i_{q,eq}^* + \tilde{i}_q^* \quad (67)$$

The switching control can be expressed as

$$\tilde{i}_q^* = i_{q1} + i_{q2} \quad (68)$$

where

$$i_{q1} = -W_w \text{sgn}(s_w) \quad (69)$$

$$i_{q2} = \begin{cases} -\lambda |s_0|^p \text{sgn}(s_{wr}) & |s_{wr}| > |s_0| \\ -\lambda |s_{wr}|^p \text{sgn}(s_q) & |s_{wr}| \leq |s_0| \end{cases}$$

The sufficient condition for finite time convergence to the sliding manifold can be described as

$$W_{wr} > \frac{\Psi_{wr}}{\Gamma_m} \quad (70)$$

$$\lambda_w^2 \geq \frac{4\Psi_{wr}}{\Gamma_m^2} \frac{\Gamma_M(W_{wr} + \Psi_{wr})}{\Gamma_m(W_{wr} - \Psi_{wr})} \quad (71)$$

$$0 < p \leq 0.5 \quad (72)$$

By selecting $p = 0.5$, we can reach the switching control as

$$\tilde{i}_q^* = -\lambda_w |s_{wr}|^{1/2} \text{sgn}(s_{wr}) - W_{wr} \int \text{sgn}(s_{wr}) dt \quad (73)$$

6. Computer simulation studies

To demonstrate the effectiveness and robustness of the proposed control approaches, MATLAB computer simulation studies have been conducted for implementing the MTPA and MPPA SMC schemes in comparison with the tradition PI-based field-oriented control for interior permanent magnet synchronous motors.

Figure 4 demonstrates the speed responses of IPM motor when the torque changes from 0 to 100 Nm at $t = 3$ s and speed changes from 200 to 1200 rpm at $t = 5$ s. Higher-order SMC shows the fastest rise time, much-reduced settling time, and chattering free response, while the first-order approach shows noticeable chattering phenomenon, and the PI-based field-oriented control shows sluggish time response. The response of first-order SMC can be improved by adjusting the switching gains, but it will result in excessive chattering. It can be observed that the higher-order SMC scheme shows the best performance in achieving the fastest response time reducing the overshoot and eliminating the chattering phenomenon.

Figure 5 shows the quadrature-axis stator current response to reference-speed and load-torque changes. The first-order SMC causes chattering in tracking the speed response with the load changes and modelling uncertainties, while the higher-order SMC yields a relatively smooth response. The traditional PI-based field-oriented control have the largest q-axis currents, hence the motor drive consumes more electrical power from the battery pack.

The direct-axis current is shown in Figure 6, unlike the traditional PI-based field-oriented control, where i_d is set to be zero, MTPA and MPPA require negative i_d reference current for maximizing the torque and power output of the interior permanent magnet synchronous motor.

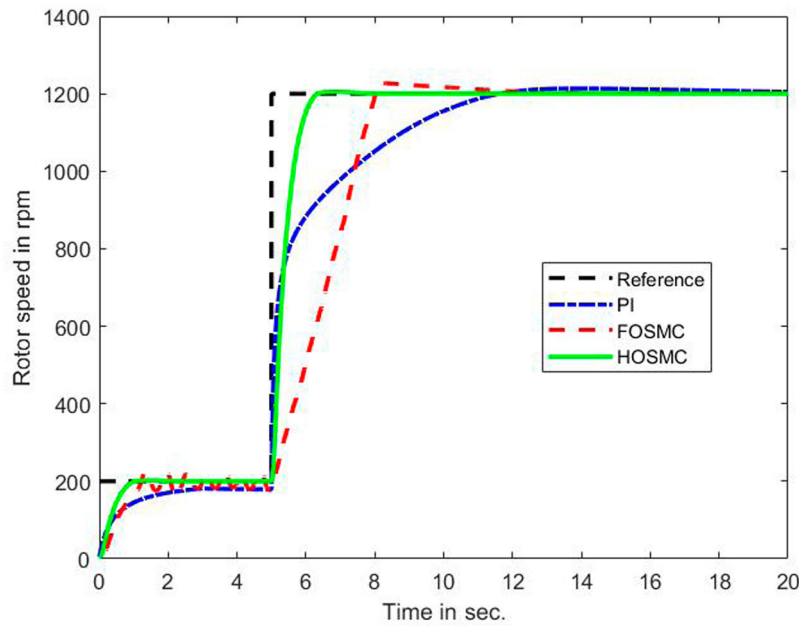


Figure 4. IPM rotor speed comparisons.

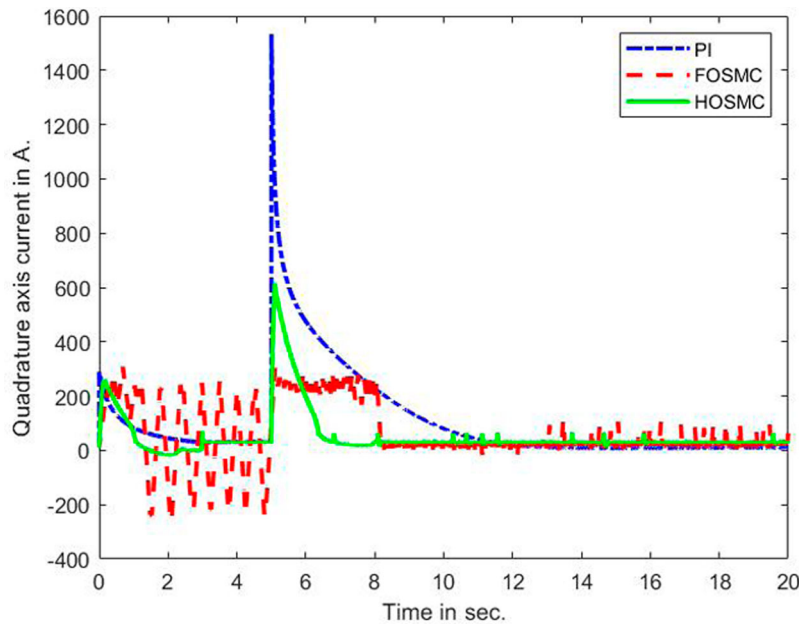


Figure 5. Quadrature axis current i_q comparisons.

The higher-order SMC again shows superior performance over the first-order method by eliminating chattering phenomenon.

Figure 7 shows the MTPA trajectory with direct-axis current i_d on x -axis and quadrature axis current i_q on y -axis.

When the load torque changes, both first-order and higher-order SMC show faster transient responses in comparison with the traditional PI-based field-oriented control scheme. Again, the higher-order SMC reaches the steady-state much faster than the first-order method.

The traditional PI-based field-oriented control shows the slowest response time. Both first-order and super-twisting-based second-order controllers show excellent performance, during speed and load torque changes, while the second-order controller demonstrates superior performance in eliminating the chattering phenomenon. On the other hand, the traditional PI controller produces unsatisfactory results under load torque changing and extraneous disturbance conditions, as the gain parameters K_p and K_i need to be adjusted in accordance with changing load and external disturbances.

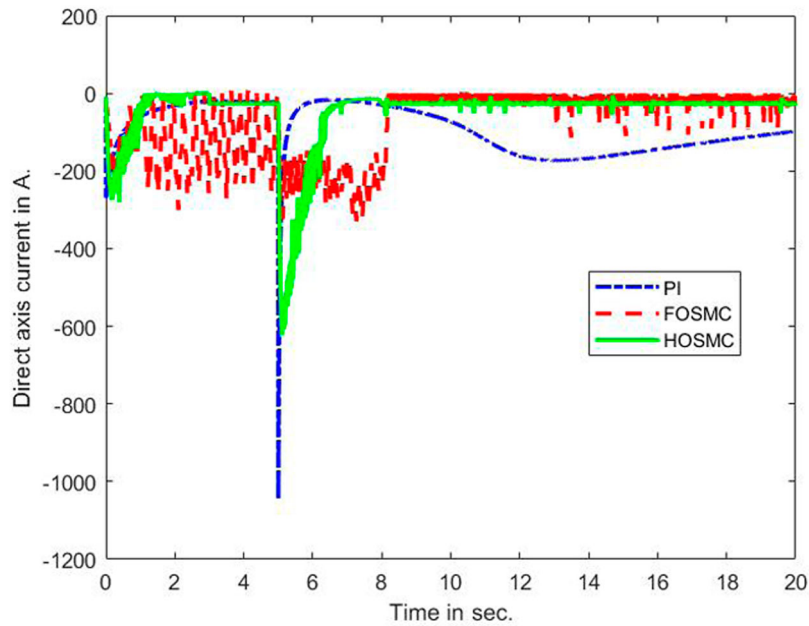


Figure 6. Direct-axis current i_d comparisons.

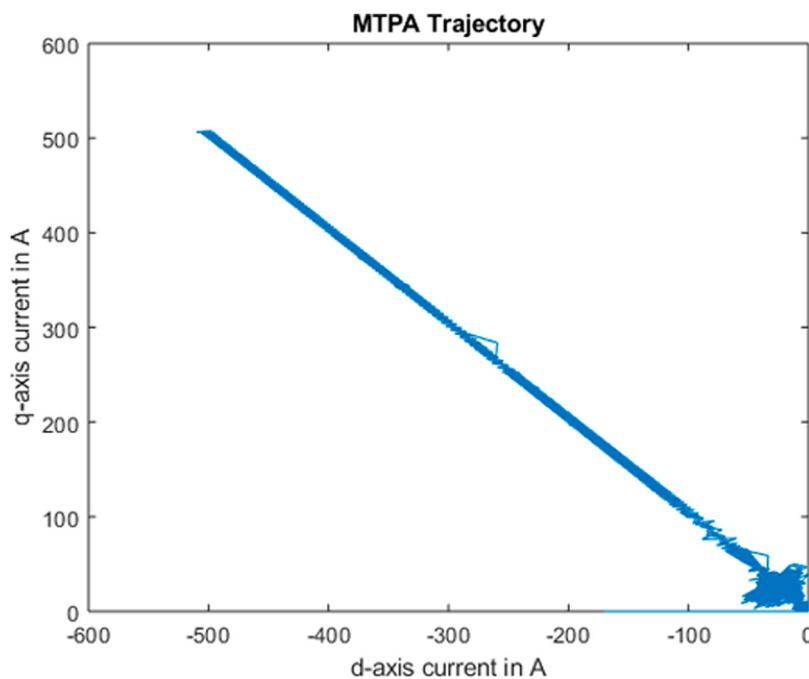


Figure 7. MTPA trajectory.

7. Conclusions and future work

In this paper, the interior permanent magnet synchronous motors have been modelled in dq synchronous rotating coordinate frame. The direct-axis reference current equation has been derived for MTPA and MPPA performance. Novel sliding-mode-based MTPA and MPPA control approaches for interior permanent magnet synchronous motor have been developed and examined, which have shown superior performance over traditional

PI-based field-oriented control. The super-twisting-based second-order SMC shows superior performance over the first-order method, in providing faster transient responses, shorter settling time, and eliminating the chattering phenomenon. For future research work, the proposed control schemes will be applied for electrified vehicle applications to improve the torque/speed regulation, the overall driving experience, controllability, safety and efficiency.

Disclosure statement

No potential conflict of interest was reported by the author(s).

References

- Alnami, H., Pang, C., Papineni, A., & Wang, X. (2021, November). Optimal interior mounted permanent magnet synchronous motors MTPA and MPPA control based on sliding mode approaches. In *Proc. of the 2021 ASME international mechanical engineering congress and exposition (IMECE)*, on-line, 2021, IMECE2021-70904.
- Krause, P., Wasynczuk, O., Sudhoff, S., & Pekarek, S. (2013, June). *Analysis of electric machinery and drive systems* (3rd ed.). IEEE Press.
- Levant, A., & Fridman, L. (2002). Higher order sliding modes. In In J. P. Barbot and W. Perruquetti, *Sliding mode control in engineering* (pp. 53–101). Marcel Dekker.
- Morimoto, S., Hatanaka, K., Tong, Y., Takeda, Y., & Hirasu, T. (1993, April). Servo drive system and control characteristics of salient pole permanent magnet synchronous motor. *IEEE Transactions on Industry Applications*, 29(2), 338–343. <https://doi.org/10.1109/28.216541>
- Morimoto, S., Hatanaka, K., Tong, Y., Takeda, Y., & Hirasu, T. (1994, October). Loss minimization control of permanent magnet synchronous motor drives. *IEEE Transactions on Industry Applications*, 41(5), 920–926. <https://doi.org/10.1109/28.297908>
- Morimoto, S., Sanada, M., & Takeda, Y. (1994, August). Wide-Speed operation of interior permanent magnet synchronous motors with high-performance current regulator. *IEEE Transactions on Industry Applications*, 30(4), 511–517. <https://doi.org/10.1109/28.297908>
- Morimoto, S., Takeda, Y., & Hirasu, T. (1990a, April). Current phase control methods for permanent magnet synchronous motors. *IEEE Transactions on Power Electronics*, 5(2), 133–139. <https://doi.org/10.1109/63.53150>
- Morimoto, S., Takeda, Y., & Hirasu, T. (1990b, October). Expansion of operating limits for permanent magnet motor by current vector control considering inverter capacity. *IEEE Transactions on Industry Applications*, 26(5), 866–871. <https://doi.org/10.1109/28.60058>
- Uddin, M. N., Radwan, T. S., & Rahman, M. A. (2002, March). Performance of interior permanent magnet drive over wide speed range. *IEEE Transactions on Energy Conversion*, 17(1), 79–84. <https://doi.org/10.1109/60.986441>
- Utkin, V., Young, K., & Ozguner, U. (1999, May). A control engineer's guide to sliding mode control. *IEEE Transactions on Control Systems Technology*, 7(3), 328–342. <https://doi.org/10.1109/87.761053>
- Wang, X., Reitz, M., & Gu, P. (2016, June). (2016). Robust sliding mode control of permanent magnet synchronous motor drive. In: *Proc. of the 2016 IEEE Transportation electrification conference & expo*. Dearborn, MI, June 27–29.
- Wang, X., Reitz, M., & Yaz, E. E. (2018, November). Field oriented sliding mode control of surface-mounted permanent magnet AC motors: theory and applications to electrified vehicles. *IEEE Transactions on Vehicular Technology*, 67(11), 10343–10356. <https://doi.org/10.1109/TVT.2018.2865905>
- Xu, Z., & Rahman, M. F. (2003, November). Sensorless sliding mode control of an interior permanent magnet synchronous motor based on extended Kalman filter. *The Fifth International Conference on Power Electronics and Drive Systems* (Vol. 1, pp. 722–727). Singapore.